



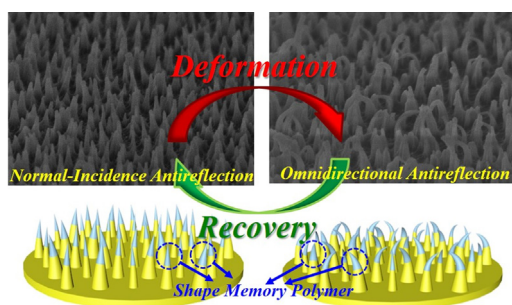
# Omnidirectional / Unidirectional Antireflection-Switchable Structures Inspired by Dragonfly Wings



Ru-Yu Chen, Chung-Jui Lai, You-Jie Chen, Mei-Xuan Wu, Hongta Yang\*

Department of Chemical Engineering, National Chung Hsing University, 145 Xingda Road, Taichung City 40227, Taiwan

## GRAPHICAL ABSTRACT



## ARTICLE INFO

### Article history:

Received 3 November 2021

Revised 29 November 2021

Accepted 4 December 2021

Available online 8 December 2021

### Keywords:

Inclined conical structures

Dragonfly wings

Shape memory polymer

Omnidirectional antireflection

Switchable

## ABSTRACT

Randomly arranged irregular inclined conical structure-covered dragonfly wings, distinguished from periodic conical structure-covered cicada wings, are with high optical transparency for wide viewing angles. Bioinspired by the antireflective structures, we develop a colloidal lithography approach for engineering randomly arranged irregular conical structures with shape memory polymer-based tips. The structures establish a gradual refractive index transition to suppresses optical reflection in the visible spectrum. By manipulating the configuration of structure tips through applying common solvent stimulations or contact pressures under ambient conditions, the resulting unidirectional antireflection and omnidirectional antireflection performances are able to be instantaneously and reversibly switched. The dependences of structure shape, structure inclination, structure arrangement, and structure composition on the switchable antireflection capability are also systematically investigated in this study.

© 2021 Elsevier Inc. All rights reserved.

## 1. Introduction

Thanks to high toughness, low density, high chemical resistance, rapid processability, and high degree of design freedom, transparent plastics have been widely utilized, substituted for inorganic materials, in a variety of advanced optical components across defense, automotive, illumination, and consumer/healthcare goods industries [1–4]. Take spectacle lenses as an example, the high mechanical stability and potential weight saving from using

polymers, instead of glass, are of significant benefits from a safety, durability, and comfort perspective. The considerable design freedom and processability of polymers further provide them with more radical design and cost efficiency in applications. One primary limitation of the transparent polymer optics however, is their inherent high refractive index, which leads to Fresnel reflection occurring on the polymer surfaces [5–6]. The light reflection, accompanied by undesired energy loss, veil glare, and ghost images, degrades overall performances of diverse optical applications [7–9]. To improve their optical transparencies and image readabilities, quarter-wavelength single-layer/multilayer interfer-

\* Corresponding author.

ence coatings with appropriate thicknesses and low refractive indices are commonly deposited onto the polymer components to diminish the refractive index difference between air and polymer [10–11]. Nevertheless, the uncommon low-refractive-index coating materials are costly. To address the issues, nanoporous antireflection coatings have been developed by numerous methodologies, including multilayer deposition of nanoparticles/hollow particles, sol–gel process, plasma-enhanced chemical vapor deposition, and phase separation [12–17]. The integration of homogeneously distributed subwavelength voids, possesses demanded low refractive indices. Unfortunately, it is still challenged for establishing a refractive index gradient, thereby the antireflection coatings are limited by narrow operating wavelengths.

Over four billion years of successive improvement through natural selection, natural creatures have provided diverse strategies to overcome versatile survival challenges [18–20]. For instance, camouflage by hawk moth wings, glasswing butterfly wings, and cicada wings, requires high optical transparency to prevent tracking by predatory birds [21–23]. The insects make use of hexagonally non-close-packed subwavelength conical structures found on their wings to generate refractive index gradients for suppressing Fresnel reflection in the visible light region as well as minimalizing light scattering. Fascinatingly, blue-tailed forest hawk dragonfly wings can even surmount the dazzle caused by sunlight during flight [24–25]. Their wing membranes are covered with subwavelength inclined conical structures, which are irregular positioning and with a broad structure size distribution. The unique structure configuration effectively moderates refractive index transitions over wide incident angles, possessing omnidirectional antireflection behaviors.

Inspired by the natural creatures, a variety of submicrometer-scale conical structures, pyramid-like structures, dome-shaped structures, pillar-shaped structures, and so on have been extensively utilized as antireflective structures during the past few decades [26–30]. The bio-inspired structures are capable of reducing unwanted reflective losses at normal incidence efficaciously. However, the optical transparencies of the structure-covered substrates are greatly impaired with the increase of viewing angle. Despite the fact that omnidirectional antireflective properties can be ameliorated by introducing submicrometer-scale inclined structures, it is arduous to design and develop the structures adopting existing photolithography-based methodologies, nanoimprinting technologies, and scanning probe lithography methods [31–33]. Benefiting from the considerable advancements in bottom-up technologies in recent years, colloidal lithography approaches render a straightforward alternative to develop high-resolution antireflective structures [34]. A colloidal monolayer is deposited onto a selected substrate to function as etching masks for patterning demanded structures under varied etching parameters. Nevertheless, most accessible deposition technologies, such as Langmuir-Blodgett technique, are restricted to low throughput. Moreover, only hexagonally close-packed colloids are available to maintain their thermodynamic stabilities, while the arrangement is not favored for constructing inclined structures. Fueled by the prompt progress of bottom-up technologies, a microfabrication-compatible spin-coating technique is recently developed to deposit non-close-packed colloidal templates, which shall provide more inter-structure space for biomimicking the inclined structures on dragonfly wings [35].

Nowadays, switchable antireflection coatings have attracted great attention in a diversity of intelligent optical devices, including lenses, sensors, dichroic mirrors, vehicle windows, display screens, etc. [36]. The structure configuration of reversibly deformable submicrometer-scale structures can be alternated between a deformed state and a recovered state to switch their corresponding antireflective properties in response to external stimuli. To achieve

the switchable antireflection functionalities, hydrogels and elastomers have been investigated for use because of their high elasticity [37–38]. Unfortunately, the temporarily deformed elastic materials-based structure configurations can only be sustained shortly under ambient conditions, that significantly restricts their long-term applications. By contrast, the temporary shape memory polymer configurations can be well-retained and return to their original configurations by applying lasers, heat, electric fields, magnetic fields, oxidation–reduction potentials, and solvents [39–44]. Benefiting from that distinct behavior, diversified antireflective structures are able to be temporarily deformed and recovered at will to reversibly switch their corresponding antireflection characteristics. Even though most shape memory polymers are with reliable manufacturability and high shape deformability, the shape recoveries triggered by physical stimuli take time and patience, while the chemicals and specific solvents, required to realize chemical stimuli-responsive shape recoveries, pose environmental hazards or cause corrosion damage to device components. Moreover, only few researches report efforts towards on-off switchable antireflection coatings, whereas unidirectional antireflection-omnidirectional antireflection switchable functionalities have not yet been achieved.

Herein, the consistency between the surface morphologies and the antireflection behavior of blue-tailed forest hawk dragonfly wings is explicated adequately. Take the dragonfly as a prototype, we design and build intelligent conical structures with stimuli-responsive shape memory polymer-based tips, capable of reversibly switching between a slightly inclined configuration and a seriously inclined configuration simply regulated by applying either contact pressures or exposure to common solvents under ambient conditions. Contrary to thermo-responsive shape memory polymers, heat is not required for both structure deformation and recovery steps. In addition, the temporarily deformed structures can be well-retained after removing the external stimuli. Importantly, the interdisciplinary integration of the dragonfly wing-inspired antireflective structures and the shape memory polymers provides a platform to realize unidirectional antireflection-omnidirectional antireflection switchable functionalities. In this study, the antireflective characteristics of disparate inclined structures are systematically investigated for bridging the bio-inspired structures and practical applications[45].

## 2. Experimental section

**Two-Dimensional Randomly Arranged Silica Colloids and Non-Close-Packed Silica Colloidal Crystals Formed by Spin-Coating.** Monodisperse Stöber silica colloids with synthetically tunable diameters (180, 130, and 80 nm) are well-dispersed in a mixture of photocurable ethylene glycol diacrylate (EGDA, Sartmer Company Corporation) monomers and ethoxylated trimethylolpropane triacrylate (ETPTA, Sartomer Company Corporation) monomers utilizing an ultrasonicator (300VT, BioLogics Incorporation). The volume fractions of silica colloids, EGDA monomers, and ETPTA monomers in the suspension are adjusted to be 20 vol%, 60 vol%, and 20 vol%, respectively. After adding 2-hydroxy-2-methyl-1-phenyl-1-propanone (BASF Corporation) as an initiator, the silica colloidal suspension is uniformly spread onto a commercial poly(ethylene terephthalate) (PET, Resound Technology Incorporation) substrate. A spin coater (EDC-650-8B, Laurell Technologies Corporation) is then employed to shear align the silica colloids at a spin speed of 7500 rpm for 8 min. Afterwards, the monomers are photopolymerized in a UV curing system (XLite 500, OPAS UV Curing Corporation) to create two-dimensional silica colloid-coated PET substrates.

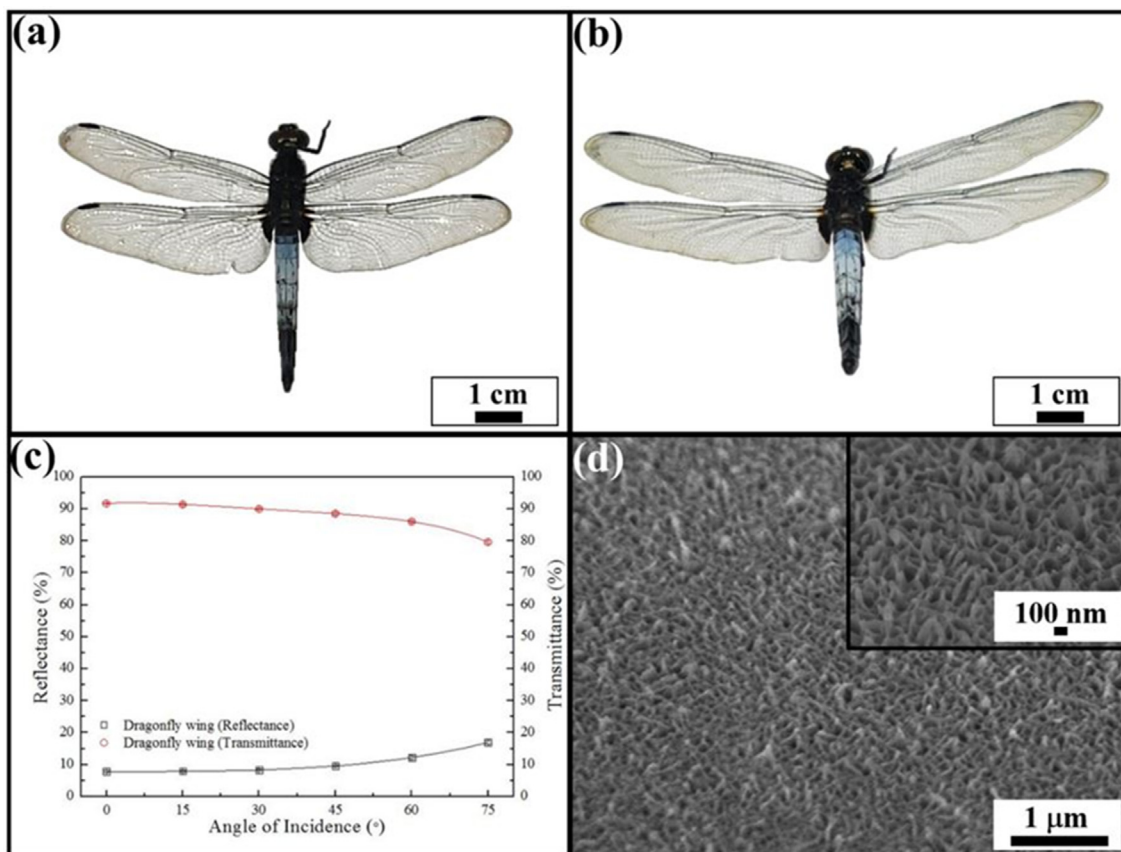


Fig. 1. Dragonfly images photographed at (a) 0 and (b) 45. (c) Average reflectances and transmittances of the dragonfly wing in the visible spectrum taken from different angles of incidence. (d) SEM image of the dragonfly wing.

**Templating Fabrication of Submicrometer-Scale Conical Structures by Colloidal Lithography.** Submicrometer-scale conical structures with high structural tunability are fabricated through reactive ion etching (RIE) of two-dimensional silica colloid-coated PET substrates on an oxygen/argon inductively coupled plasma-reactive ion etcher (PlasmaPro 100 Polaris, Oxford Instruments Public Listed Company). The oxygen/argon ( $O_2/Ar$ ) flow rates vary from 10/5 to 20/5 sccm, with a constant process pressure (15 mTorr) and a constant ICP power density (50 W) for varied durations from 5 to 12.5 min. After the colloidal lithographic patterning, the silica templates remained attached to the conical structures are removed using hydrofluoric acid (3 vol%), followed by drying at room temperature.

**Characterization.** Photographs and microscopic features of the samples are observed using a digital camera (ZV-1, Sony Public Listed Company) and a FEG-scanning electron microscopy (JSM-7500F, JEOL Biotechnology Company Limited), respectively. Before SEM imaging, the samples are sputtered with a gold layer by a sputter coater (Cressington 108, Ted Pella Incorporation). Optical reflection and transmission spectra of the samples are analyzed by employing an ultraviolet-visible-near-infrared spectrometer (HR4000, Ocean Optics Incorporation) with a halogen-tungsten lamp as power source. Average reflectances and transmittances in the visible spectrum (380–750 nm) are performed from 7 different spots of each sample.

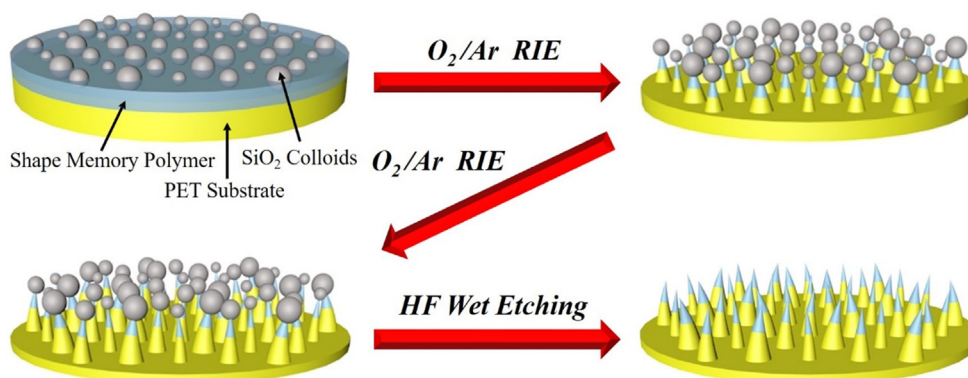
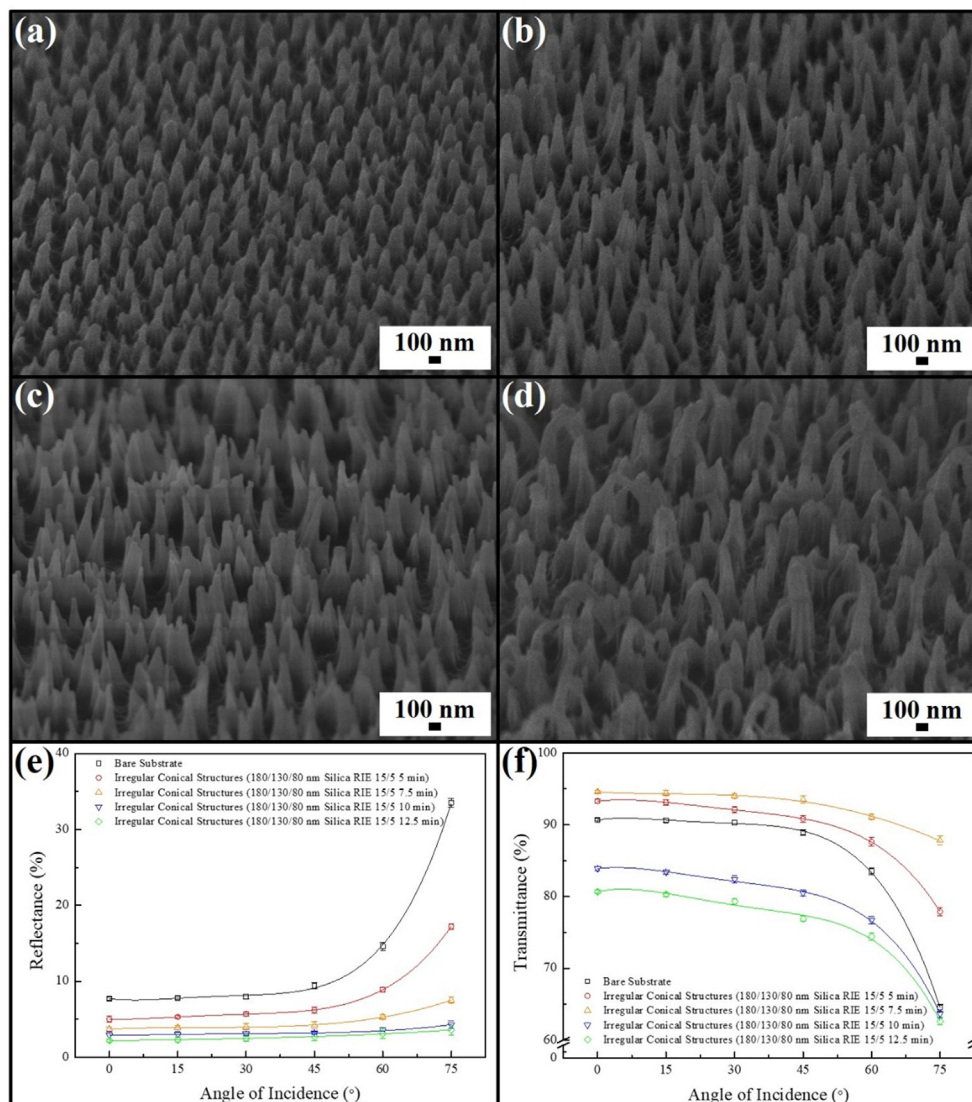


Fig. 2. Schematic of deformable irregular antireflective structures inspired by dragonfly wings.



**Fig. 3.** SEM images of deformable irregular conical structures templated from randomly arranged 180/130/80 nm silica colloids after reactive ion etching ( $O_2$  (15 sccm)/Ar (5 sccm)) for (a) 5 min, (b) 7.5 min, (c) 10 min, and (d) 12.5 min. (e) Average reflectances and (f) transmittances of the deformable irregular conical structures in the visible spectrum taken from different angles of incidence.

### 3. Results and discussion

Blue-tailed forest hawk dragonfly (*Orthetrum triangulare*), belonging to the Libellulidae family found in Asian, is renowned for its azure bluish abdomen and highly transparent wings for large viewing angles (Fig. 1 (a) and (b)). Different from cicada wings, pellucid hawk moth (*Cephonodes hylas*) wings and so forth, the dragonfly wings display notable broadband omnidirectional antireflection performance [46–47]. The average reflectance and transmittance in the visible spectrum (380 to 750 nm) of the dragonfly wing are only increased by 8% and decreased by 9%, respectively, as the angle of incidence varies from  $0^\circ$  to  $75^\circ$  (Fig. 1 (c)). Such behavior is attributed to submicrometer-scale inclined conical structures covering the wing membranes (Fig. 1 (d)). Fascinatingly, the inclined structures are separated from each other and irregularly positioning, which are distinct from previously reported periodic antireflective structures [48]. The randomness is not only showing on the structure arrangement, but also the structure size, which is with a base diameter distribution varied from 80 and 180 nm.

Inspired by the dragonfly wings, a standard microfabrication-compatible spin-coating technology and a colloidal lithographic patterning methodology are integrated to fabricate irregular conical structures in this study (Fig. 2). In the fabrication procedures, a monolayer of randomly arranged silica colloid/poly(EGDA)/poly(ETPTA) composite is spin-coating onto a commercial PET substrate. During the coating process, a thin poly(EGDA)/poly(ETPTA) copolymer wetting layer ( $\sim 100$  nm), possessing room temperature shape processability, is created between the monolayer silica colloids and the PET substrate [49–50]. With a high reactive ion etching selectivity between silica and polymers, the silica colloids function as templates to preserve the shape memory polymer and the PET substrate underneath them in an  $O_2$ /Ar RIE process. After wet etching the silica templates, randomly arranged irregular conical structures are engineered. It is worth mentioning that the conical structure configuration can be easily determined through tuning RIE parameters.

To mimic the irregular conical structures on the dragonfly wings, 180/130/80 nm silica spherical colloids with an amount ratio of 1:2:1 are spin-coated onto a PET substrate. The shape

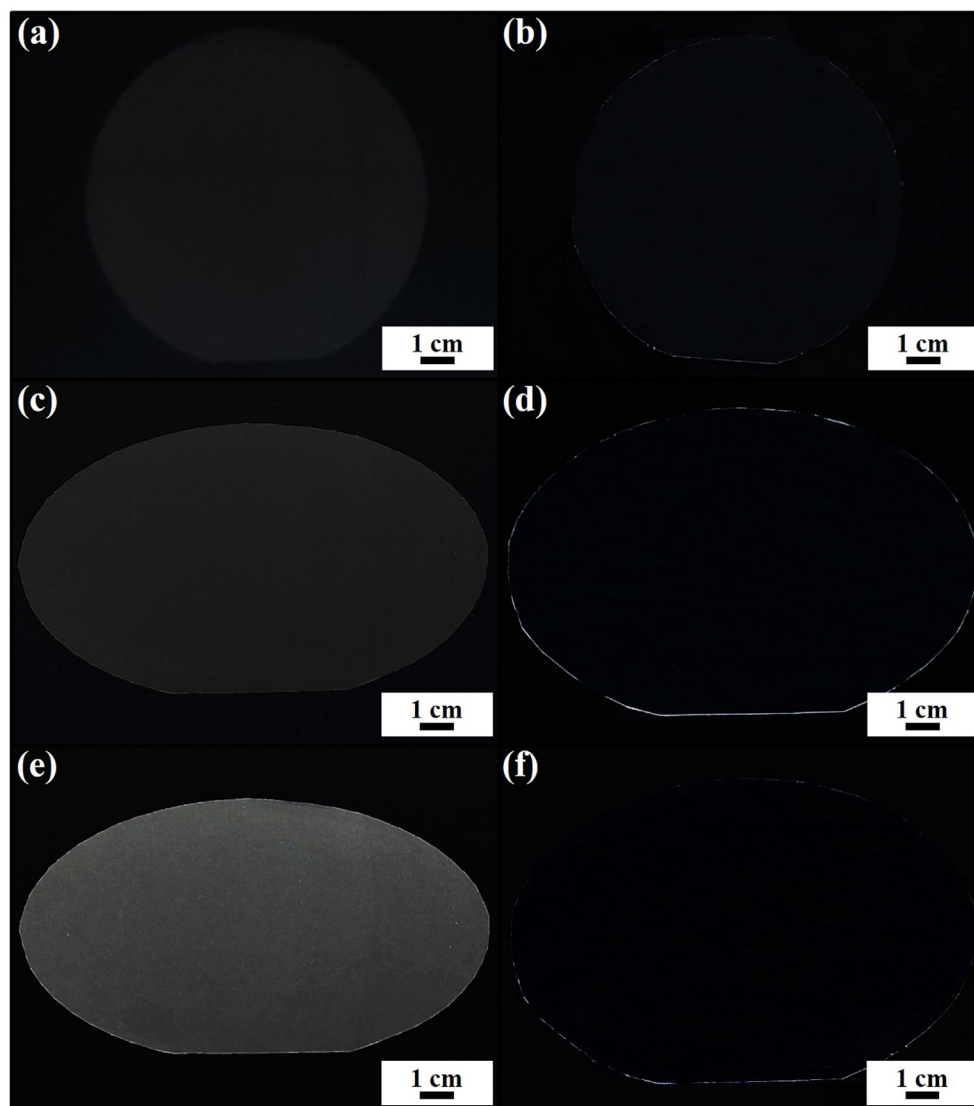


**Fig. 4.** PET substrate images photographed at (a), (b) 0°; (c), (d) 30°; (e), (f) 60°. The PET substrate in (a), (c), and (e) is featureless, while the PET substrate in (b), (d), and (f) is coated with deformable irregular conical structures ( $O_2$  (15 sccm)/Ar (5 sccm), 7.5-min RIE).

memory polymer embedded silica colloids are irregularly positioning and  $\sim 100$  nm apart from neighboring colloids in the colloidal monolayer (Figure S1). The polymer part of the two-dimensional silica template-covered PET substrate is then selectively etched with  $O_2$  (15 sccm) and Ar (5 sccm) for 5 to 12.5 min, respectively. Importantly, the combination of isotropic  $O_2$  RIE and anisotropic Ar RIE leads to the formation of polymeric conical structures consisting of shape memory polymer tops and PET bottoms (Fig. 2). After removing the silica etching masks, randomly arranged conical structures with base diameters of 180, 130, and 80 nm are patterning on the substrate directly. Owing to the silica etching masks do no shrink under the RIE treatments, it is clear that longer RIE treatments bring about the constitution of higher conical structures with sharper tips (Fig. 3 (a)–(d)). Fascinatingly, the sharp tips can't fully support the above silica colloids as RIE duration reaches 7.5 min, and therefore slightly bend in random directions. It is worthy to note that the random arrangement of silica templates creates ample inter-structural space to engineer inclined structures, in contrast to most self-assembled close-packed colloid templates. The structure tips are getting sharper and the resultant structures

are further bended as the RIE duration extends beyond 10 min. On account of van der Waals forces among neighboring inclined structures with larger heights, the structures are randomly bunched to form large-area collapsed bundles [51]. To investigate broadband omnidirectional antireflective properties of the as-fabricated structures, average reflectances and average transmittances in the visible spectrum of the structure-covered substrates are taken from varied incident and detection angles (Fig. 3 (e) and (f)). It is found that the average reflectance of the bare substrate (black curve) greatly increased from 8% to 33% as the angle incident increases from 0° to 75°. In comparison with that, the optical reflections can be effectively suppressed by introducing the irregular structures to establish smooth refractive index transitions on substrate surfaces at varied incident angles. Higher inclined conical structure-covered substrates therefore exhibit lower average reflectances and higher average transmittances, even for large incident angles. Surprisingly, even though average reflectances of the conical structure-covered substrates with 10-min and 12.5-min RIE treatments (blue/green curves) remain less than 5% for whole the angles of incidence, the corresponding average transmittances

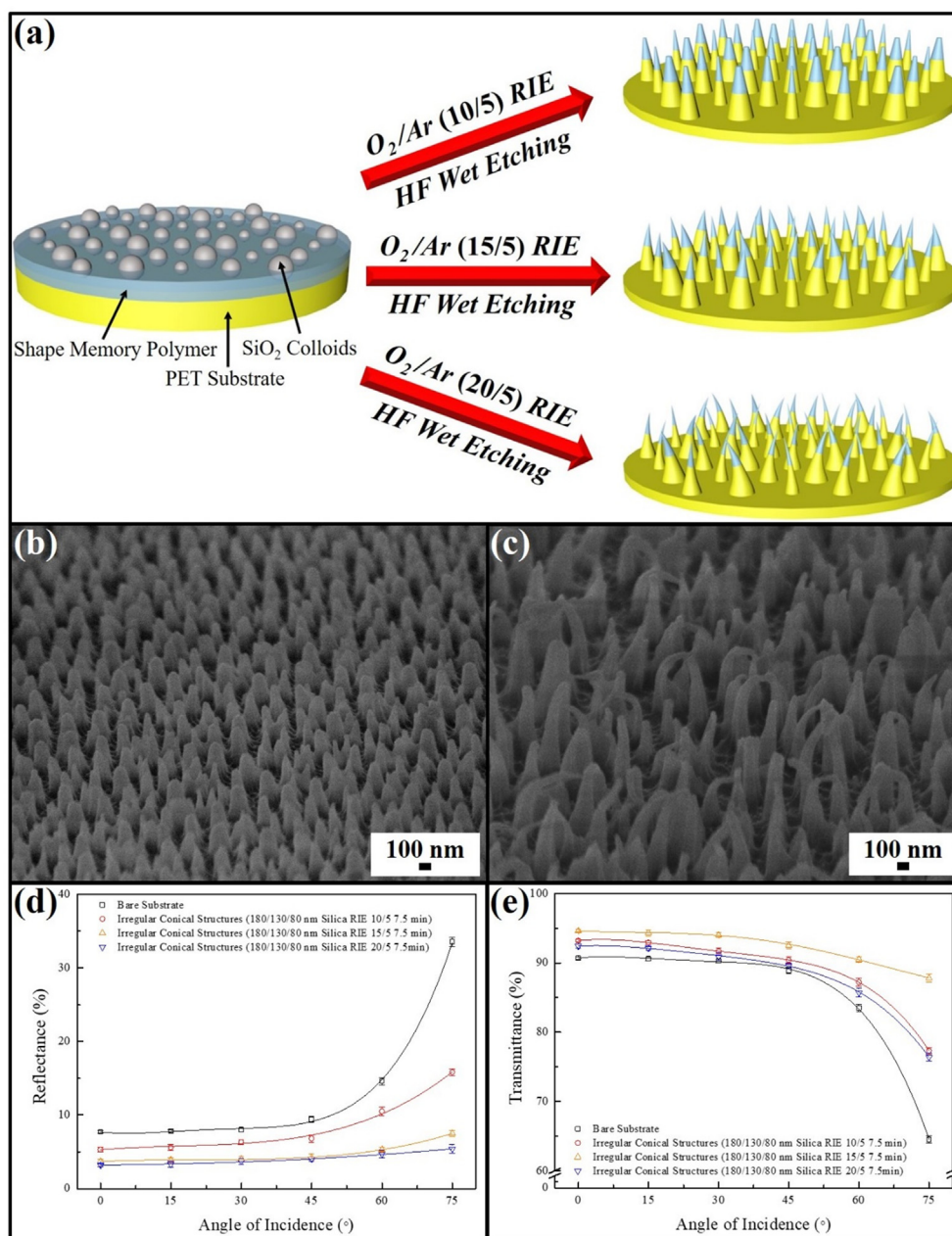


**Fig. 5.** (a) Schematic of fabrication strategies for deformable irregular antireflective structures with varied reactive ion etching parameters. SEM images of irregular conical structures templated from randomly arranged 180/130/80 nm silica colloids after reactive ion etching for 7.5 min using O<sub>2</sub>/Ar gases with varied flow rates of (b) 10/5 sccm, and (c) 20/5 sccm. (e) Average reflectances and (f) transmittances of the irregular conical structures in the visible spectrum taken from different angles of incidence.

are significantly decreased with increasing incident angles. The impaired optical transmittances are induced by Rayleigh scattering by the resulting micrometer-scale bundled structures. Last but not least, the unbundled inclined conical structures with 7–5-min RIE treatment behave impressive antireflection performance, which is comparable with that of dragonfly wings (Fig. 1 (c)). The average transmittance (orange curve) merely decreased from 94% to 88% even as the angle of incidence varies from 0° to 75°. The PET substrate images photographed at 0°, 30°, and 60° further confirm that the irregular inclined conical structures can be introduced to greatly suppress the Fresnel's reflection greatly (Fig. 4). Clearly, the bare substrate turns milky as the viewing angle reaches 60°, while the irregular conical structure-covered substrate remains highly transparent.

The dependence of structure configuration on antireflection characteristics is also investigated through tuning etching gas flow rates to create conical structures with varied inclinations (Fig. 5 (a)). The O<sub>2</sub>/Ar flow rates vary from 10/5 to 20/5 sccm. Instead of conical features, hump-like structures with nearly vertical side-walls are constructed in the presence of weak isotropic etching (O<sub>2</sub> (10 sccm)) (Fig. 5 (b)). Obviously, the structure base diameter remains unchanged, while the structures become higher and sharper under higher O<sub>2</sub> flow rate. It is apparent that the sharp conical structures can not support the above silica templates, hence they are seriously inclined and entangled with each other as the O<sub>2</sub> flow rate reaches 20 sccm (Fig. 5 (c)). Although the intertwined inclined conical structure-covered substrate displays low average reflectances over wide angles of incidence, this substrate behaves even

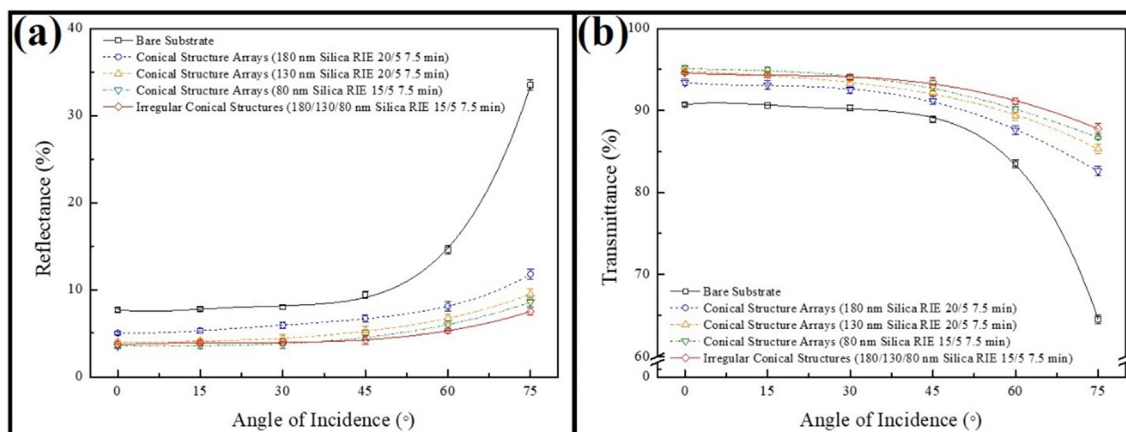


**Fig. 6.** (a) Average reflectances and (b) transmittances of conical structures templated from 180 nm silica colloidal crystals ( $O_2$  (20 sccm)/Ar (5 sccm), 7.5-min RIE), 130 nm silica colloidal crystals ( $O_2$  (20 sccm)/Ar (5 sccm), 7.5-min RIE), 80 nm silica colloidal crystals ( $O_2$  (15 sccm)/Ar (5 sccm), 7.5-min RIE), and 180/130/80 nm silica colloids ( $O_2$  (15 sccm)/Ar (5 sccm), 7.5-min RIE) in the visible spectrum taken from different angles of incidence.

lower average transmittances than those of hump-like structure-covered substrate (Fig. 5 (d) and (e)). It is believed that part of incident light is internally refracted or reflected within the entangled conical structure tips, leading to the diminished transparency. The results indicate that the intertwined conical structures are incapable of greatly enhancing omnidirectional antireflection properties.

In addition to the structure inclination, arrangements of antireflective structures play an important role in their antireflection performances. To gain a better comprehension of the structure arrangement effect, spin-coated silica colloidal monolayers are utilized as etching masks to pattern periodic conical structures (Figure S2). Instead of randomly arranged silica colloids, the self-assembled 180 nm silica colloidal crystals, 130 nm silica colloidal crystals, and 80 nm silica colloidal crystals are hexagonally non-close-packed (Figure S3). Similar to the previous results, the conical structure arrays templated from the silica colloidal crystals are slightly inclined after 7.5-min RIE treatments ( $O_2$  (15 sccm)/Ar (5 sccm)), resulting in enhanced omnidirectional antireflection characteristics (Figure S4, Figure S5, and Figure S6). In contrast, the high conical structures fabricated by 10-min or 12.5-min RIE treatments are bunched into micrometer-scale bundles, bringing about scattering of visible light. Afterwards, 7.5-min RIE treatments with different etching gas flow rates are applied to build periodic conical structures with varied structure inclinations (Figure S7). Unanticipatedly, the conical structure arrays templated from 180 nm silica colloidal crystals display their lowest average reflectances and highest transmittances as the  $O_2$ /Ar flow rates reach 20/5 sccm, respectively, instead of 15/5 sccm (Figure S8). The ample inter-structure spacing ( $\sim 1.4D$ , where  $D$  indicates the diameter of silica colloids) allows the formation of seriously inclined conical structure array without any bunched structures. Similar evolution trends can also be found on the conical structure arrays templated from non-close-packed 130 nm silica colloidal crystals (Figure S9). Interestingly, as a result of insufficient inter-structure spacing, micrometer-scale conical shape aggregates are generated by applying non-close-packed 80 nm silica colloidal crystals as etching masks in the presence of  $O_2$  (20 sccm) and Ar (5 sccm) (Figure S10). The conical structure arrays therefore exhibit their lowest average reflectances and highest transmittances as the  $O_2$ /Ar flow rates achieve 15/5 sccm, respectively. Importantly, compared with these optical properties of the most appropriate inclined conical structure arrays templated from non-close-packed colloidal crystals, the irregular inclined conical structures templated from ran-

domly arranged colloids exhibit even lower average reflectances and higher average transmittances for wide incident angles (Fig. 6). The results disclose that broad structure size distribution, optimal structure height, and sufficient inter-structure spacing are all critical in designing and developing broadband omnidirectional antireflective structures.

The poly(EGDA)/poly(ETPTA) composite-based conical structure tips ( $\sim 100$  nm in height) can be deformed and recover their original shapes in response to external stimuli at room temperature [52,53]. The distinctive shape memory functionality allows structural transitions between slightly inclined conical structures and seriously inclined conical structures to realize switchable unidirectional/omnidirectional antireflection performance. Above-mentioned slightly inclined conical structure-substrate, templated from randomly arranged 180/130/80 nm silica colloids with a 7.5-min RIE treatment ( $O_2$  (15 sccm)/Ar (5 sccm)), is immersed in water, and then dried under ambient conditions (Fig. 7). It is observed that the configuration of the PET-based bottoms is well-retained, while the shape memory polymer-based structure tips are seriously inclined after drying out of water. The increase in structure inclination is induced by water evaporation-derived capillary force, which is larger than the shape memory polymer elasticity. The randomly arranged irregular conical structures provide adequate space between neighboring structures for creating inclined structures without bunched structures. Importantly, the temporarily deformed structures are recovered in an ethanol drying procedure. The shape memory polymers can absorb ethanol to relax stretched polymer chains and to increase their mobility. As a result of the weak capillary force produced by ethanol evaporation, the resulting entropy elasticity of polymer chains is capable of recovering the seriously inclined conical structures to their original slightly inclined conical structures after drying out of ethanol [54,55]. Surprisingly, the appearances of the original structure-covered substrate, deformed structure-covered substrate, and recovered structure-covered substrate are not able to be identified as different. Average reflectances and average transmittances of the structure-cover substrates during the shape memory recovery are conducted at varied angles of incidence to evaluate their corresponding antireflection characteristics (Fig. 7 (g) and (h)). It is found that these structures possess indistinguishable antireflection performances at normal incidence. More surprisingly, the deformed conical structures behave the lowest average reflectance and the highest average transmittance at  $60^\circ$  and  $75^\circ$ . The seriously inclined conical structures in the deformed

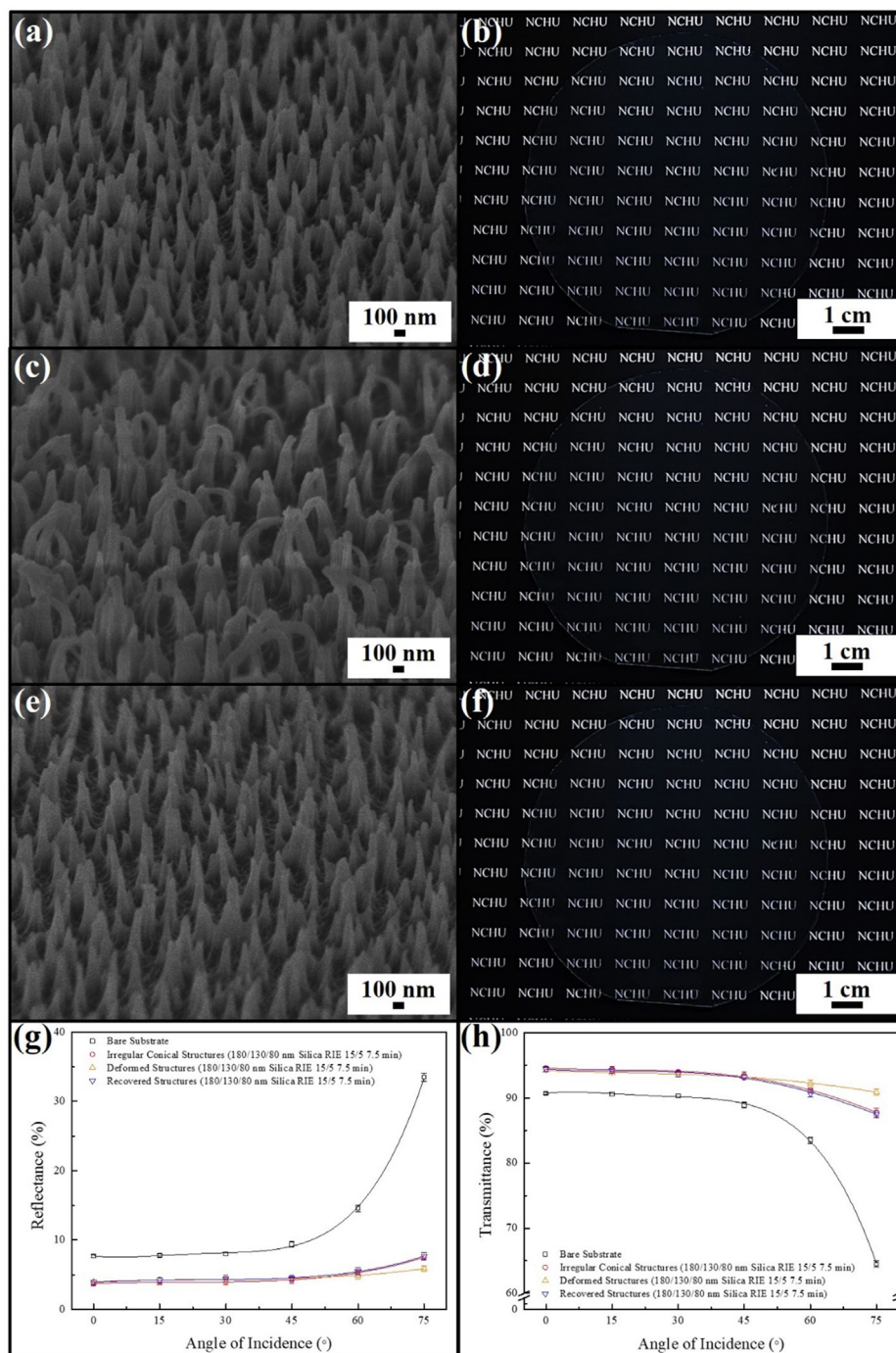


**Fig. 7.** (a) SEM image and (b) photographic image of the deformable irregular conical structures ( $O_2$  (15 sccm)/Ar (5 sccm), 7.5-min RIE). (c) SEM image and (d) photographic image of the deformed irregular conical structures ( $O_2$  (15 sccm)/Ar (5 sccm), 7.5-min RIE). (e) SEM image and (f) photographic image of the recovered irregular conical structures ( $O_2$  (15 sccm)/Ar (5 sccm), 7.5-min RIE). (g) Average reflectances and (h) average transmittances of the irregular conical structures (original state/deformed state/recovered state) in the visible spectrum taken from different angles of incidence.

state establish even smoother refractive index transitions at large incident angles, which further improve their omnidirectional antireflection performance. The findings indicate that unidirectional antireflection and omnidirectional antireflection performances are able to be switched by applying common solvents on the irregular PET-based conical structures with shape memory polymer tips.

For further increasing the inclination of deformed structures, 180/130/80 nm silica colloidal monolayer is spin-coated onto a

shape memory polymer-coated PET substrate, followed by etching treatments to pattern whole shape memory polymer-based conical structures (Figure S11). The as-fabricated structures are slightly inclined, and are similar in antireflection characteristics to the irregular PET-based conical structures. In sharp contrast, the conical structures are wholly bended and bunched into bundled structures after drying out of water under ambient conditions (Figure S12). The capillary force-induced destructive structure-covered substrate therefore turns milky in appearance, caused by

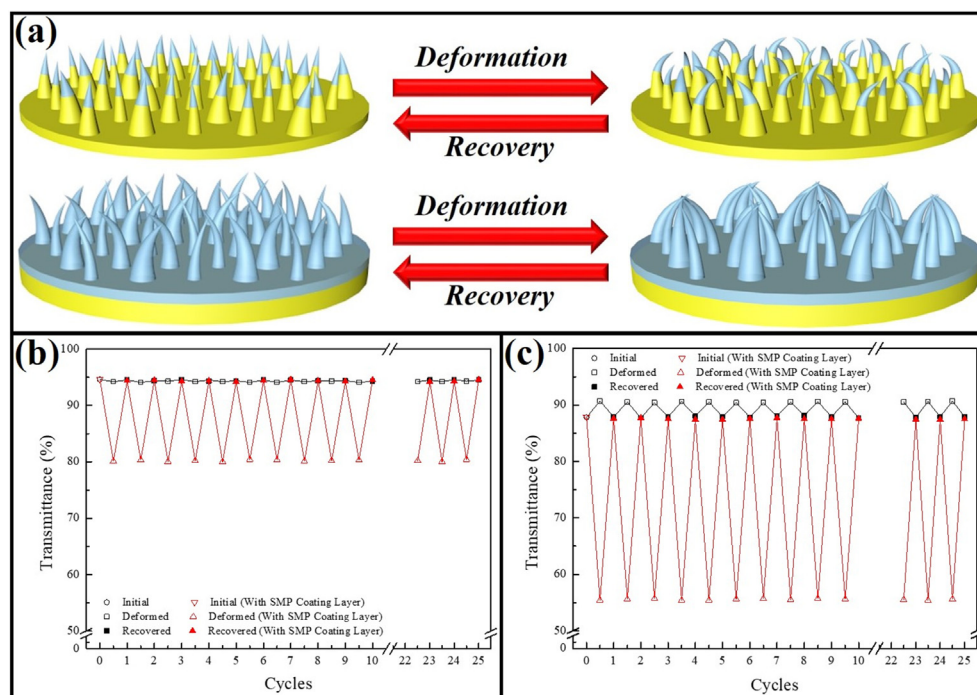


**Fig. 8.** (a) Schematic of deformation and recovery processes for deformable irregular conical structures and temporarily destructible irregular conical structures. Average transmittances of the deformable irregular conical structures and the temporarily destructible irregular conical structures in the deformation/recovery cycle stimulated by applying solvents in the visible spectrum taken from (b) 0°, and (c) 75°.

light scattering. Although the formation of destructive structures leads to low average reflectances and transmittances at all the incident angles, the temporarily destructible structures and their optical properties are fully recovered in tens of seconds in an ethanol drying procedure. The results suggest that the irregular shape memory polymer-based conical structures provide a controllable on–off switch for antireflection functionalities triggered by external solvent stimulations. Importantly, drastically different antireflection performances in the deformed state are realized by engineering irregular conical structures with varied proportions of shape memory polymers (Fig. 8 (a)). The substrate covered with irregular shape memory polymer-based conical structures (temporarily destructible structures) in the deformed state display lower average transmittance at 0°, and even lower average transmittance at 75° (Fig. 8 (b) and (c)). On the contrary, the optical transparency of the substrate covered with irregular PET-based conical structures with shape memory polymer tips (temporarily deformable structures) remains unchanged at 0° in the shape memory cycle, whereas its antireflection performance is even improved in the deformed state at 75°. Most importantly, both shape memory cycles are reversible, while the corresponding optical transparencies are smoothly transformed for more than 25 cycles.

Besides solvent stimulations, the structural recovery can be triggered by applying normal forces on deformed structures and bundled structures directly. The external contact pressures can be transferred and stored in the stretched shape memory polymer chains, which are with a low glass transition temperature. The increase in internal energy can overcome the shape memory activation barrier, and therefore allow the temporarily deformed structures to recover immediately. To affirm the con-

tact pressure-enabled shape memory recovery, different standard test weights are placed onto the temporarily deformed structures. The substrate is covered with a piece of cover glass before pressurizing to ensure varied contact pressures are applied on the deformed structures evenly. As verified in Fig. 9 (a)–(d), more deformed structures are recovered, and the recovered structures are with lower structure inclinations under higher contact pressures. In addition, it is found that slightly inclined conical structures are obtained after applying a contact pressure of 2.94 N/cm<sup>2</sup>. Moreover, its corresponding optical properties match well with those of undeformed structures, indicating that the temporarily deformed structures are fully recovered. It is worthwhile to emphasize that even if the structures under varied contact pressures exhibit similar antireflection characteristics for small incident angles, the antireflection capability is gradually reduced with the increase of contact pressures (Fig. 9 (e) and (f)). The average reflectance is increased from 5% to 8%, and the average transmittance is decreased from 91% to 87% at 75° as the applied contact pressure reaches 2.94 N/cm<sup>2</sup>. The findings disclose that the antireflection functionality of the irregular PET-based conical structures with shape memory polymer tips is tunable by applying varied contact pressures. By contrast, the irregular shape memory polymer-based conical structures display opposite antireflection trends during the pressure-induced shape recovery (Figure S13). The introducing of higher contact pressures on the structure bundles significantly improves their omnidirectional antireflection performances. As evidenced previously, both contact pressure-induced shape memory cycles are reversible. Deteriorations of the antireflective properties are not recognized even after 25 shape memory cycles (Fig. 10).

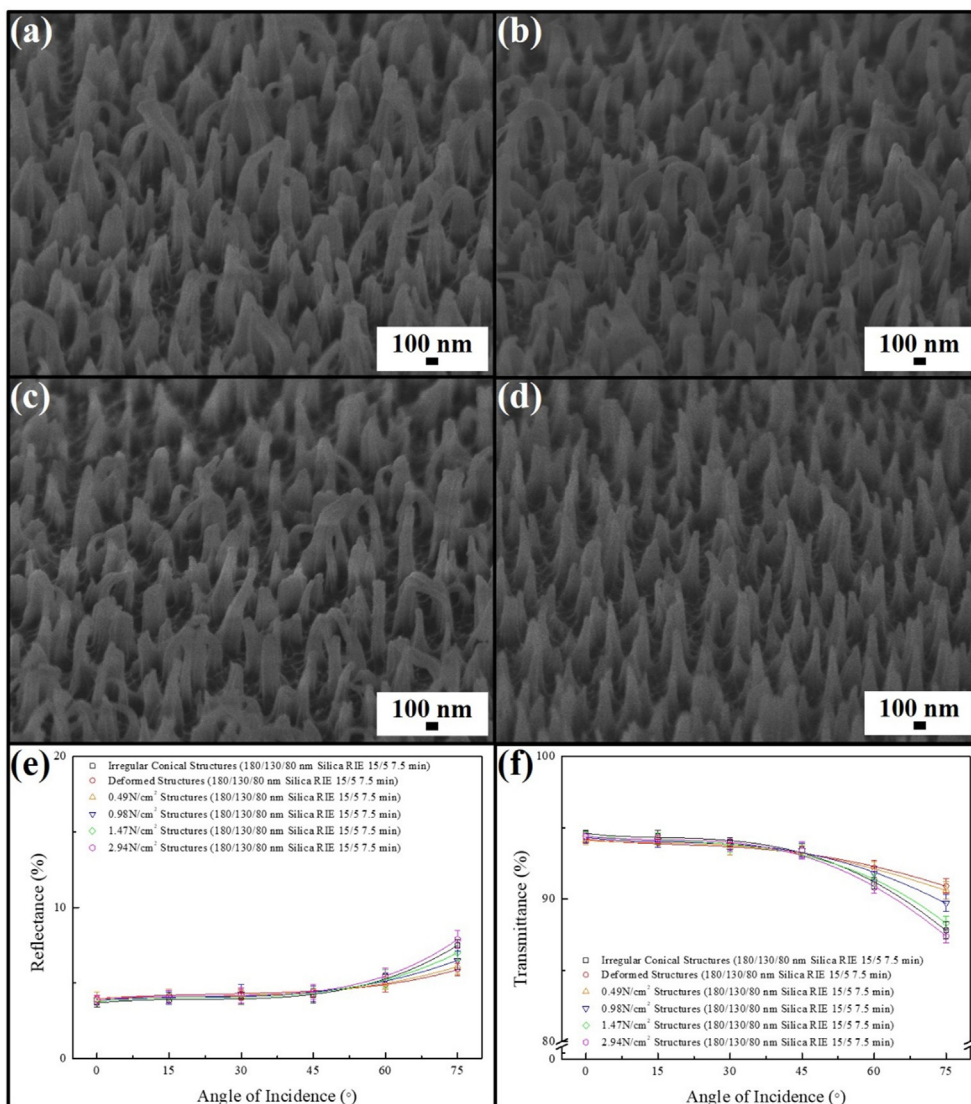


**Fig. 9.** SEM images of the temporarily deformable irregular conical structures (O<sub>2</sub> (15 sccm)/Ar (5 sccm), 7.5-min RIE) after applying varied contact pressures of (a) 0.49 N/cm<sup>2</sup>, (b) 0.98 N/cm<sup>2</sup>, (c) 1.47 N/cm<sup>2</sup> and (d) 2.94 N/cm<sup>2</sup>. (e) Average reflectances and (f) transmittances of the deformable irregular conical structures after applying contact pressure stimulations in the visible spectrum taken from different angles of incidence.

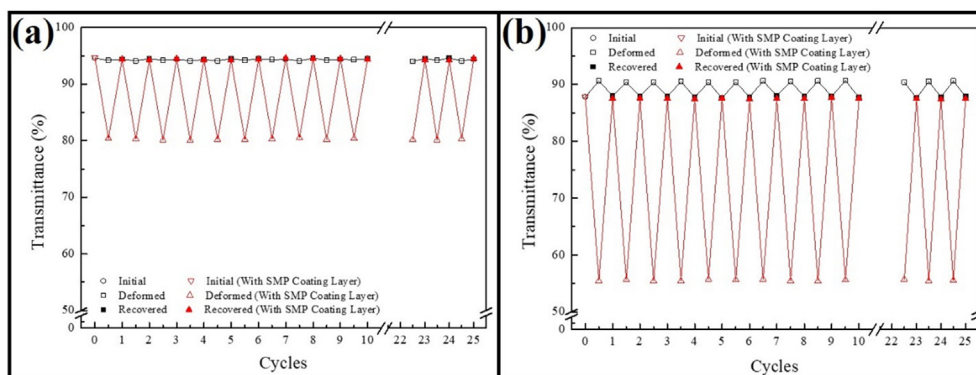


**Fig. 10.** Average transmittances of the deformable irregular conical structures and the temporarily destructible irregular conical structures in the deformation/recovery cycle stimulated by applying contact pressures in the visible spectrum taken from (b) 0°, and (c) 75°.

#### 4. Conclusions

To conclude, randomly arranged irregular conical structures with stimuli-responsive shape memory polymer-based tips are engineered by combining a spin-coating technique with a colloidal lithography technology. Compared to non-close-packed conical structure arrays, the randomly arranged conical structures exhibit lower average reflectances and higher average transmittance in the visible spectrum. Importantly, the structure tips are bended after drying out of water, leading to the formation of seriously inclined conical structures with a random arrangement. The seriously inclined structures create gradual refractive index transitions at varied incident angles, resulting in an improved broadband omnidirectional antireflection performance. Besides solvent stimulations, the antireflection characteristics can be recovered by applying contact pressures under ambient conditions. The findings disclose that these structures behave a reversibly unidirectional/omnidirectional antireflection-switchable functionality. Interestingly, drastically different switchable antireflection performances are also realized by fabricating irregular conical structures with varied proportions of shape memory polymers. The as-developed methodologies create novel dimensions for a wide range of existing and future optical devices.

#### CRediT authorship contribution statement

**Ru-Yu Chen:** Methodology, Writing – original draft. **Chung-Jui Lai:** Writing – original draft. **You-Jie Chen:** Writing – original draft. **Mei-Xuan Wu:** Writing – original draft. **Hongta Yang:** Conceptualization, Writing – review & editing, Supervision, Project administration, Funding acquisition.

#### Declaration of Competing Interest

The authors declare that they have no known competing financial interests or personal relationships that could have appeared to influence the work reported in this paper.

#### Acknowledgments

This study is financially supported by the National Science Council (Grant No. MOST 110-2221-E-005-050-MY2). The authors gratefully acknowledge the use of Field Emission Scanning Electron Microscope belonging to the Instrument Center of National Chung Hsing University.

#### Appendix A. Supplementary material

Supplementary data to this article can be found online at <https://doi.org/10.1016/j.jcis.2021.12.025>.

#### References

- [1] T. Peršak, B. Viltušnik, J. Hernavs, S. Klančnik, Vision-Based Sorting Systems for Transparent Plastic Granulate, *Appl. Sci. (Basel)* 10 (12) (2020) 4269, <https://doi.org/10.3390/app10124269>.
- [2] N. Yamada, R. Ino, H. Tomura, Y. Kondo, Y. Ninomiya, High-Mobility Transparent p-Type CuI Semiconducting Layers Fabricated on Flexible Plastic Sheets: Toward Flexible Transparent Electronics, *Adv. Electron. Mater.* 3 (2017) 6.
- [3] S.Y. Huang, X.F. Xu, Optical Chirality Detection Using a Topological Insulator Transistor, *Adv. Opt. Mater.* 9 (2021) 7.
- [4] K.X. Chen, Y. Hou, S.Q. Chen, D. Yuan, H.P. Ye, G.F. Zhou, Design, Fabrication, and Applications of Liquid Crystal Microlenses, *Adv. Opt. Mater.* 9 (2021) 2100370.
- [5] A. D'Arco, V. Mussi, S. Petrov, S. Tofani, M. Petrarca, R. Beccherelli, D. Dimitrov, V. Marinova, S. Lupi, D.C. Zografopoulos, Fabrication and spectroscopic characterization of graphene transparent electrodes on flexible cyclo-olefin

- substrates for terahertz electro-optic applications, *Nanotechnology* 31 (36) (2020) 364006, <https://doi.org/10.1088/1361-6528/ab96e6>.
- [6] A. Calabria, I. Molina, S.G. Jin, Soil Moisture Content from GNSS Reflectometry Using Dielectric Permittivity from Fresnel Reflection Coefficients, *Remote Sens.* 12 (2020) 1.
- [7] J.J. Zhou, X.P. Hao, J. Song, C.Y. Xie, Y. Liu, X. Wang, Stray light separation based on the changeable veiling glare index for the vacuum radiance temperature standard facility, *Opt. Express* 29 (2021) 12344–12356.
- [8] Z.J. Li, Q. Zhao, W.L. Gong, Distorted point spread function and image reconstruction for ghost imaging, *Opt. Lasers Eng.* 139 (2021) 8.
- [9] X.H. Li, Y.X. Guo, Y.J. Ren, J.J. Peng, J.S. Liu, C. Wang, H. Zhang, Narrow-bandgap materials for optoelectronics applications, *Front. Phys.* 17 (2022) 33.
- [10] Y. Pan, D. Yin, X. Yu, N. Hao, J. Huang, Multilayer-Structured Wood Electroless Cu-Ni Composite Coatings for Electromagnetic Interference Shielding, *Coatings* 10 (8) (2020) 740, <https://doi.org/10.3390/coatings10080740>.
- [11] J. Li, W.J. Wang, R.X. Zhu, Y.X. Huang, Superhydrophobic Artificial Compound Eye with High Transparency, *ACS Appl. Mater. Interfaces* 13 (2021) 35026–35037.
- [12] D.T. Vu, H.-W. Chiu, R. Nababan, Q.M. Le, S.-W. Kuo, L.-K. Chau, C.-C. Ting, H.-C. Kan, C.-C. Hsu, Enhancing Upconversion Luminescence Emission of Rare Earth Nanophosphors in Aqueous Solution with Thousands Fold Enhancement Factor by Low Refractive Index Resonant Waveguide Grating, *ACS Photon.* 5 (8) (2018) 3263–3271.
- [13] C. Kauppinen, K. Isakov, M. Sönanen, Grass-like Alumina with Low Refractive Index for Scalable, Broadband, Omnidirectional Antireflection Coatings on Glass Using Atomic Layer Deposition, *ACS Appl. Mater. Interfaces* 9 (2017) 15038–15043.
- [14] S. Kim, J.H. Park, Chemically Robust Antifog Nanocoating through Multilayer Deposition of Silica Composite Nanofilms, *ACS Appl. Mater. Interfaces* 12 (37) (2020) 42109–42118.
- [15] D.M. Lin, X.R. Zeng, H.Q. Li, X.J. Lai, T.Y. Wu, One-pot fabrication of superhydrophobic and flame-retardant coatings on cotton fabrics via sol-gel reaction, *J. Colloid Interface Sci.* 533 (2019) 198–206.
- [16] Y. Zhou, Q. Li, B. Dang, Y. Yang, T. Shao, H. Li, J. Hu, R. Zeng, J.L. He, Q. Wang, A Scalable, High-Throughput, and Environmentally Benign Approach to Polymer Dielectrics Exhibiting Significantly Improved Capacitive Performance at High Temperatures, *Adv. Mater.* 30 (2018) 7.
- [17] J. Kamp, S. Emonds, J. Borowec, M.A.R. Toro, M. Wessling, On the organic solvent free preparation of ultrafiltration and nanofiltration membranes using polyelectrolyte complexation in an all aqueous phase inversion process, *J. Membr. Sci.* 618 (2021) 10.
- [18] J. Lee, J. Song, J. Park, S. Yoo, Toward Ultra-Efficient OLEDs: Approaches Based on Low Refractive Index Materials, *Adv. Opt. Mater.* 9 (2021) 12.
- [19] Y.B. Jin, B. Djafari-Rouhani, D. Torrent, Gradient index phononic crystals and metamaterials, *Nanophotonics* 8 (2019) 685–701.
- [20] F.T. Chi, Y.Y. Zeng, C. Liu, N. Pan, C.C. Ding, F.C. Yi, Highly stable self-cleaning antireflection coatings from fluoropolymer brush grafted silica nanoparticles, *Appl. Surf. Sci.* 507 (2020) 7.
- [21] A. Papadopoulos, E. Skoulas, A. Mimidis, G. Perrakis, G. Kenanakis, G.D. Tsiibidis, E. Stratakis, Biomimetic Omnidirectional Antireflective Glass via Direct Ultrafast Laser Nanostructuring, *Adv. Mater.* 31 (2019) 8.
- [22] Z.W. Han, Z. Wang, B. Li, X.M. Feng, Z.B. Jiao, J.Q. Zhang, J. Zhao, S.C. Niu, L.Q. Ren, Flexible Self-Cleaning Broadband Antireflective Film Inspired by the Transparent Cicada Wings, *ACS Appl. Mater. Interfaces* 11 (2019) 17019–17027.
- [23] Y.C. Lu, X. Liu, R. Hattori, C. Ren, X.W. Zhang, T. Komiyama, D. Kuzum, Ultralow Impedance Graphene Microelectrodes with High Optical Transparency for Simultaneous Deep Two-Photon Imaging in Transgenic Mice, *Adv. Funct. Mater.* 28 (2018) 9.
- [24] C. Damgaard-Carstensen, M. Thomaschewski, F. Ding, S.I. Bozhevolnyi, Electrical Tuning of Fresnel Lens in Reflection, *ACS Photon.* 8 (2021) 1576–1581.
- [25] M.L. De Marco, T.Z. Jiang, J. Fang, S. Lacomme, Y.B. Zheng, A. Baron, B.A. Korgel, P. Barois, G.L. Drisko, C. Aymonier, Broadband Forward Light Scattering by Architectural Design of Core-Shell Silicon Particles, *Adv. Funct. Mater.* 31 (2021) 11.
- [26] Y. Yamada, H. Iizuka, N. Mizoshita, Silicon Nanocone Arrays via Pattern Transfer of Mushroomlike SiO<sub>2</sub> Nanopillars for Broadband Antireflective Surfaces, *ACS Appl. Nano Mater.* 3 (2020) 4231–4240.
- [27] K. Kim, S. Yoo, J.H. Huh, Q.H. Park, S. Lee, Limitations and Opportunities for Optical Metafluids To Achieve an Unnatural Refractive Index, *ACS Photon.* 4 (2017) 2298–2311.
- [28] X.Q. Lin, Y.Y. Liu, K. Wang, C. Wei, W. Zhang, Y.L. Yan, Y.J. Li, J.N. Yao, Y.S. Zhao, Two-Dimensional Pyramid-like WS<sub>2</sub> Layered Structures for Highly Efficient Edge Second-Harmonic Generation, *ACS Nano* 12 (2018) 689–696.
- [29] R.E. Nowak, M. Vehse, O. Sergeev, T. Voss, M. Seyfried, K. von Maydell, C. Agert, ZnO Nanorods with Broadband Antireflective Properties for Improved Light Management in Silicon Thin-Film Solar Cells, *Adv. Opt. Mater.* 2 (2014) 94–99.
- [30] S. Rasappa, H. Hulkkonen, L. Schulte, S. Ndoni, J. Reuna, T. Salminen, T. Niemi, High molecular weight block copolymer lithography for nanofabrication of hard mask and photonic nanostructures, *J. Colloid Interface Sci.* 534 (2019) 420–429.
- [31] T.M. Garakani, M.J. Richter, A. Böker, Controlling the bio-inspired synthesis of silica, *J. Colloid Interface Sci.* 488 (2017) 322–334.
- [32] Z.J. Wang, J.G. He, B. Hu, P. Shan, Z.Y. Xiong, R.B. Su, C. He, X.M. Yang, X.F. Long, Ca<sub>2</sub>B<sub>5</sub>O<sub>9</sub>Cl and Sr<sub>2</sub>B<sub>5</sub>O<sub>9</sub>Cl: Nonlinear Optical Crystals with Deep-Ultraviolet Transparency Windows, *ACS Appl. Mater. Interfaces* 12 (2020) 4632–4637.

- [33] W.J. Wang, J. Li, R.H. Li, B.Q. Li, X.S. Mei, X.F. Sun, Fabrication of Hierarchical Micro/Nano Compound Eyes, *ACS Appl. Mater. Interfaces* 11 (2019) 34507–34516.
- [34] Y.D. Wang, M.Y. Zhang, Y.K. Lai, L.F. Chi, Advanced colloidal lithography: From patterning to applications, *Nano Today* 22 (2018) 36–61.
- [35] Utsav; Khanna, S.; Paneliya, S.; Ray, A.; Mukhopadhyay, I.; Banerjee, R. Controlled etching of silica nanospheres monolayer for template application: A systematic study. *Appl. Surf. Sci.* **2020**, *500*, 11.
- [36] H. Yan, T. Liu, K.e. Yang, B. Huang, G. Zhou, X. Jiang, Z. Zhang, L. Yan, Nanoscale etching of microporous coatings for broadband antireflection coatings, *Thin Solid Films* 698 (2020) 137858, <https://doi.org/10.1016/j.tsf.2020.137858>.
- [37] H. Hou, E. Simsek, T. Ma, N.S. Johnson, S. Qian, C. Cissé, D. Stasak, N. Al Hasan, L. Zhou, Y. Hwang, R. Radermacher, V.I. Levitas, M.J. Kramer, M.A. Zaem, A.P. Stebner, R.T. Ott, J. Cui, I. Takeuchi, Fatigue-resistant high-performance elastocaloric materials made by additive manufacturing, *Science* 366 (6469) (2019) 1116–1121.
- [38] J.R. Wang, Z. Chen, X.Y. Li, M.J. Liu, Y. Zhu, L. Jiang, Plastic-like Hydrogels with Reversible Conversion of Elasticity and Plasticity and Tunable Mechanical Properties, *ACS Appl. Mater. Interfaces* 11 (2019) 41659–41667.
- [39] C. Li, Y. Jiao, Y. Zhang, S. Jiang, X. Lv, S. Wu, J. Li, Y. Hu, J. Ye, K. Liu, D. Wu, J. Chu, Noncontact All-In-Situ Reversible Reconfiguration of Femtosecond Laser-Induced Shape Memory Magnetic Microcones for Multifunctional Liquid Droplet Manipulation and Information Encryption, *Adv. Funct. Mater* 31 (20) (2021) 2100543, <https://doi.org/10.1002/adfm.v31.2010.1002/adfm.202100543>.
- [40] S. Bhattacharya, R. Hailstone, C.L. Lewis, Thermoplastic Blend Exhibiting Shape Memory-Assisted Self-Healing Functionality, *ACS Appl. Mater. Interfaces* 12 (2020) 46733–46742.
- [41] Y. Xie, Y. Meng, W.X. Wang, E. Zhang, J.S. Leng, Q.B. Pei, Bistable and Reconfigurable Photonic Crystals-Electroactive Shape Memory Polymer Nanocomposite for Ink-Free Rewritable Paper, *Adv. Funct. Mater.* 28 (2018) 11.
- [42] C.P. Ma, S. Wu, Q.J. Ze, X. Kuang, R.D. Zhang, H.J. Qi, R.K. Zhao, Magnetic Multimaterial Printing for Multimodal Shape Transformation with Tunable Properties and Shiftable Mechanical Behaviors *ACS Appl. Mater. Interfaces* 13 (2021) 12639–12648.
- [43] Q.K. Liu, W. Wang, M.F. Reynolds, M.C. Cao, M.Z. Miskin, T.A. Arias, D.A. Muller, P.L. McEuen, I. Cohen, Micrometer-sized electrically programmable shape-memory actuators for low-power microrobotics, *Sci. Robot.* 6 (2021) 10.
- [44] Y.L. Ni, Y.F. Zhang, S.Y. Leo, Y. Fang, M.Z. Zhao, L. Yu, K.D. Schulze, W.G. Sawyer, T.E. Angelini, P. Jiang, C.R. Taylor, Unconventional Shape Memory Mechanisms of Nanoporous Polymer Photonic Crystals: Implications for Nano-Optical Coatings and Devices, *ACS Appl. Nano Mater.* 1 (2018) 6081–6090.
- [45] Stöber, W.; Fink, A.; Bohn, E. J. J. o. c.; science, i. Controlled growth of monodisperse silica spheres in the micron size range. *J. Colloid Interface Sci.* **1968**, *26*, 62–69.
- [46] Z. Wang, H.L. Ding, D.L. Liu, C.H. Xu, B. Li, S.C. Niu, J. Li, L.P. Liu, J. Zhao, J.Q. Zhang, Z.Z. Mu, Z.W. Han, L.Q. Ren, Large-Scale Bio-Inspired Flexible Antireflective Film with Scale-Insensitivity Arrays, *ACS Appl. Mater. Interfaces* 13 (2021) 23103–23112.
- [47] A. Yoshida, M. Motoyama, A. Kosaku, K. Miyamoto, Antireflective nanoprotuberance array in the transparent wing of a hawkmoth *Cephonodes hylas*, *Zool. Sci.* 14 (1997) 737–741.
- [48] Y.F. Feng, X.H. Liu, K.S. Li, F. Gong, J. Shen, Y. Lou, Glass Flow Evolution and the Mechanism of Antireflective Nanoprotuberance Arrays in Nanoholes by Direct Thermal Imprinting, *ACS Appl. Mater. Interfaces* 13 (2021) 16968–16977.
- [49] X.F. Liu, B. Choi, N. Gozubenli, P. Jiang, Periodic arrays of metal nanorings and nanocrescents fabricated by a scalable colloidal templating approach, *J. Colloid Interface Sci.* 409 (2013) 52–58.
- [50] P. Jiang, Large-scale fabrication of periodic nanostructured materials by using hexagonal non-close-packed colloidal crystals as templates, *Langmuir* 22 (9) (2006) 3955–3958.
- [51] R.R. Del Grande, A.F. Fonseca, R.B. Capaz, Energy barriers for collapsing large-diameter carbon nanotubes, *Carbon* 159 (2020) 161–165.
- [52] Y. Fang, Y.L. Ni, S.Y. Leo, B.C. Wang, V. Basile, C. Taylor, P. Jiang, Direct Writing of Three-Dimensional Macroporous Photonic Crystals on Pressure-Responsive Shape Memory Polymers, *ACS Appl. Mater. Interfaces* 7 (2015) 23650–23659.
- [53] Y. Fang, Y.L. Ni, S.Y. Leo, C. Taylor, V. Basile, P. Jiang, Reconfigurable photonic crystals enabled by pressure-responsive shape-memory polymers, *Nat. Commun.* 6 (2015) 8.
- [54] C.J. Leverant, S.Y. Leo, M.A. Cordoba, Y.F. Zhang, N. Charpota, C. Taylor, P. Jiang, Reconfigurable Anticounterfeiting Coatings Enabled by Macroporous Shape Memory Polymers, *ACS Appl. Polym. Mater.* 1 (2019) 36–46.
- [55] H. Dumlu, A. Marquardt, E. Zirdehi, F. Varnik, Y. Shen, K. Neuking, G. Eggeler, A Mechanical Analysis of Chemically Stimulated Linear Shape Memory Polymer Actuation, *Materials* 14 (3) (2021) 481, <https://doi.org/10.3390/ma14030481>.